

The structure and evolution of the northern Australian dryline

Sarah J. Arnup and Michael J. Reeder

School of Mathematical Sciences, Monash University, Australia

(Manuscript received January 2009; revised September 2009)

The diurnal cycle of the northern Australian dryline is examined through three 24-hour series of cross-sections taken from the Australian Bureau of Meteorology's Limited Area Prediction System (LAPS) forecasts during the period 13–14 October 2002. The development of the dryline is analysed within the framework of the frontogenesis function applied to the mixing ratio. Close agreement is found between the LAPS forecasts of the low-level wind field and the network of automatic weather station (AWS) and manual observations, as well as with the available Atmospheric InfraRed Sounder (AIRS) satellite images.

During the afternoon, a heat trough extending across northern Australia drives a sea-breeze circulation from the coastal side of the trough and a weak solenoidal circulation in the dry air inland of the trough. As boundary-layer turbulence subsides overnight and surface friction reduces, the low-level flow is accelerated toward low pressure, sharpening the mixing-ratio gradient in the region from just above the nocturnal boundary layer to 900 hPa. The contribution from convergence to the mixing-ratio frontogenesis reaches a maximum around midnight, while the contribution from deformation to the mixing-ratio frontogenesis reaches a maximum before sunrise as Coriolis deflection rotates the nocturnal winds and the axis of dilatation becomes aligned with the heat trough.

The diurnal cycle of the northern Australian dryline is compared with that of the dryline which develops over the Great Plains of the United States. In contrast to the Australian dryline, the Great Plains dryline is strongest during the afternoon. While boundary-layer turbulence disrupts the dryline over northern Australia, it strengthens the Great Plains dryline by drying the moist boundary layer at higher terrain elevations and transporting westerly momentum to the surface. The resulting low-level westerlies oppose low-level easterlies in the moist air leading to strong convergent mixing-ratio frontogenesis which strengthens the Great Plains dryline in the afternoon.

Introduction

The dryline is a prominent feature of the northern Australian environment. Recently, Arnup and Reeder (2007) constructed a low-level climatology of the northern Australian dryline from the Australian Bureau of Meteorology's operational Limited Area Prediction System (LAPS) (Puri et al. 1998) forecasts and automatic weather station (AWS) observations. They suggested that the dryline develops as follows: daytime surface heating produces sea-breeze circulations

near the coast and a large inland heat trough that extends east-west along northern Australia. At night, air parcels accelerate toward low pressure, increasing convergence and deformation within the heat trough. This wind field sharpens the moisture gradient across the heat trough into a dryline, especially above the surface. The dryline was found to be strongest in the early hours of the morning during spring, confirming observations taken in the southern gulf region of northern Queensland during the Gulf Line Experiment (GLEX; Goler et al. 2006; Smith et al. 2006).

An especially dramatic nocturnal rearrangement of the circulation has been identified recently as a key feature of the West African monsoon circulation (Parker et al. 2005). Here

Corresponding author address: Sarah J. Arnup, PO Box 28M, Monash University, Vic. 3800, Australia.
Email: sarah.arnup@sci.monash.edu.au

too the low-level winds are weakest in the afternoon when the convective boundary layer is deep and the winds intensify overnight when boundary-layer turbulence subsides to form a strong southwesterly nocturnal jet. Parker et al. (2005) found that this diurnal circulation plays an important role in the moisture budget over West Africa. The nocturnal jet is responsible for the advection of moisture into the African continent from the Atlantic Ocean that is subsequently mixed vertically on the following day. Furthermore, the seasonal evolution of the diurnally varying circulations have been implicated in the onset of the monsoon and the northward migration of the monsoon system (Sultan et al. 2007). Although the effect of the diurnally varying circulation on the moisture budget of northern Australia is not examined in this paper, these studies suggest that the nocturnal acceleration of moist tropical air toward the inland heat low may be an important moisture source in the region.

Arnup and Reeder (2007) focused on the low-level climatological seasonal and diurnal differences in the environment at 925 hPa, and gave less attention to the development of individual drylines. The current paper explores the evolution and structure of a typical dryline from 13–14 October 2002, focusing particularly on the vertical circulation. A comparison is made also with the well-known dryline that occurs over the Great Plains in the United States during late spring and early summer (e.g. Schaefer 1986; Miller et al. 2001).

This paper is structured as follows. Firstly, the data-sets used in this paper are described, followed by a description of the structure and evolution of the northern Australian dryline during the period 13–14 October 2002, through a series of 24-hour vertical cross-sections taken at three different locations across northern Australia. The development of the dryline is then analysed within the framework of the vector frontogenesis function derived by Keyser et al. (1988), but with mixing-ratio replacing potential temperature. The LAPS forecast is then compared with AWS observations, AIRS satellite data and radiosonde observations from Mt Isa. A comparison of the drylines over northern Australia and the Great Plains is then presented, followed by the conclusions.

Data

A network of AWSs is maintained by the Bureau of Meteorology over Australia and surrounding islands. Manual observations are taken also at remote outstations. Together, these stations provide high quality, regular observations of temperature, moisture, wind, pressure and precipitation (see Fig. 12(a) for AWS and manual observation locations). However, the horizontal coverage provided by these stations is very sparse over the northern and central regions of Australia, which are the regions on which the present study focuses. For this reason, the analyses in this paper are based mainly on the Bureau of Meteorology's operational Limited Area Weather Prediction System, LAPS (Puri et al. 1998), with the observations serving mainly as a check for the model results.

LAPS is a combined numerical forecast model and objective analysis scheme with a horizontal resolution of 0.375° . The forecast model is based on the hydrostatic primitive equations in sigma (σ) coordinates, where $\sigma = p/p_s$ (p is the pressure at any given level and p_s is the surface pressure), and includes a prognostic equation for the surface temperature, as well as parametrisations of the boundary-layer physics, large-scale and convective precipitation, and radiation. Every six hours LAPS assimilates surface synoptic measurements, ship and drifting-buoy reports, radiosonde and upper-level wind observations, satellite sounding data from the Television Infra-Red Observation Satellite Operational Vertical Sounder, Geostationary Meteorological Satellite cloud-drift winds, and single-level winds from aircraft reports. The initial conditions are interpolated from the Bureau of Meteorology's lower-resolution Global Analysis and Prediction system (GASP), and consequently are relatively featureless. Only after a few hours of integration does the mesoscale structure emerge strongly in LAPS.

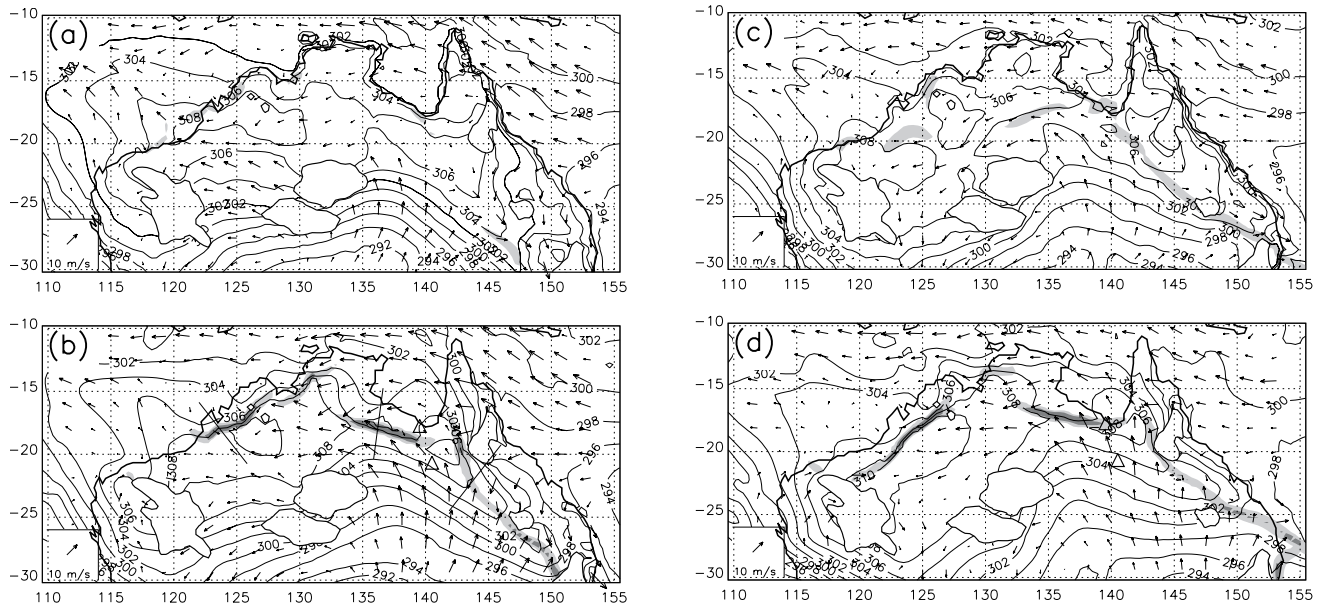
The 0.375° LAPS forecasts were used by Arnup and Reeder (2007) to construct their low-level climatologies. Since the climatology includes the period 13–14 October 2002, the 0.375° LAPS forecasts have been used in this case study to allow for comparison with previous work. The period 13–14 October was chosen as it coincides with GLEX (Goler et al. 2006; Smith et al. 2006), which provided additional observations of the southern Gulf region of northern Queensland to validate the LAPS forecast.

Where available, data from the Atmospheric InfraRed Sounder (AIRS; Standard Retrieval Product with HBS Version 5) are used also to verify the moisture fields within the LAPS three-hour forecasts. AIRS measures upwelling radiance over 2378 bands in the thermal infrared spectrum and the ranges selected allow the determination of atmospheric temperature to 1°C per 1 km thickness layer and relative humidity to 20 per cent per 2 km thickness layer (NASA 2008). The retrieved data are used to derive three-dimensional maps of air and surface temperature, water vapour, and cloud properties.

The diurnal cycle of the dryline

The low-level environment over northern Australia during the period 13–14 October shows a typical spring day and is similar to the spring climatology described by Arnup and Reeder (2007). The most striking feature is the sharp moisture gradient, which strengthens overnight to form a dryline and subsequently erodes during the day (Fig. 1). The exact magnitude of the mixing-ratio gradient depends upon the resolution of the model, and the term dryline is used because the mixing-ratio gradient intensifies dramatically. The potential temperature maximum in the northwest of the continent and the secondary maximum located southeast of the Gulf of Carpentaria in northern Queensland form the western and eastern ends of a heat trough that extends across northern Australia (Fandry and Leslie 1984; Kepert and Smith 1992; Adams 1993; Spengler et al. 2005). The dryline is located in this heat trough.

Fig. 1 Mixing-ratio gradient, potential temperature (contour interval 2 K) and winds at 925 hPa. Light shading indicates mixing-ratio gradient greater than $4 \times 10^{-5} \text{ g kg}^{-1} \text{ m}^{-1}$, dark shading indicates greater than $8 \times 10^{-5} \text{ g kg}^{-1} \text{ m}^{-1}$. (a) 1300 EST (1100 WST) 13 October 2002. (b) 0100 EST (2300 WST) 14 (13) October 2002. (c) 1300 EST (1100 WST) 14 October 2002. (d) 0100 EST (2300 WST) 15 (14) October 2002. The three black lines in (b) indicate the locations of vertical cross-sections (eastern, northern and western) taken across the dryline (see Figs 2 – 9). The triangles in (d) mark the location of AWS time series Burketown on the Gulf coast and Cloncurry inland from the Gulf (see Fig. 11). The ordinate is longitude in degrees and the abscissa is latitude in degrees. The blank areas enclosed with solid dark lines indicate topography above 500 m.



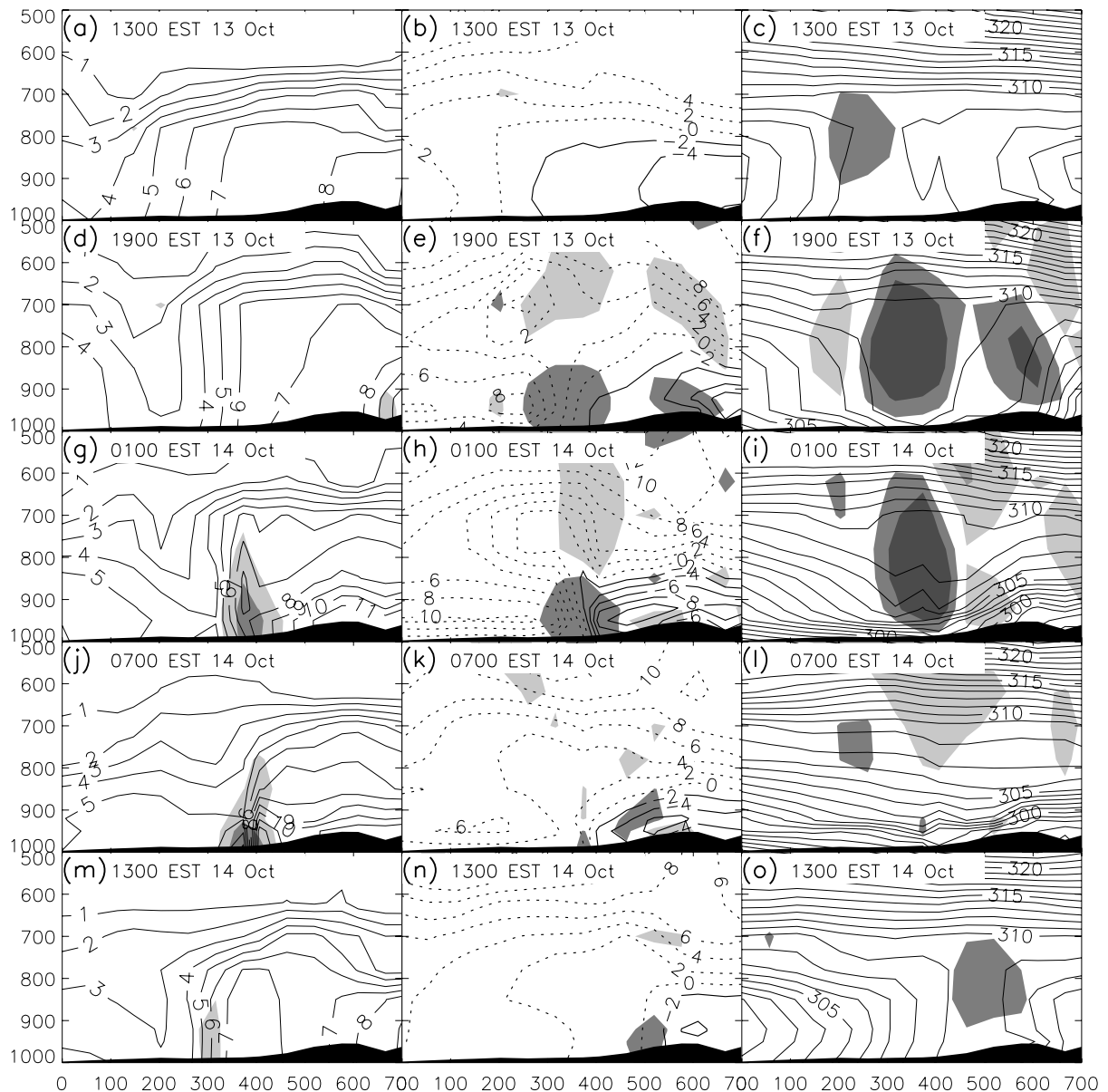
Arnup and Reeder (2007) found that at night air parcels accelerate toward low pressure, increasing low-level convergence and deformation within the heat trough. This sharpens the moisture gradient across the tropical and continental air mass boundary into a dryline within the heat trough. To further examine the roles of the inland heat trough, the sea-breeze and the nocturnal acceleration of the low-level winds in the development and evolution of the dryline, a series of vertical cross-sections from the surface to 500 hPa is presented in this paper for a continuous 24-hour LAPS forecast. The locations of the cross-sections are marked in Fig. 1(b).

As the present study focuses on the diurnal cycle, the relevant time is the local time. However, there are three time zones in Australia (not including Central Western Time), with the Australian Eastern Standard Time (EST; UTC+10) and Australian Western Standard Time (WST; UTC+8) zones differing by two hours. The third time zone is the Australian Central Standard Time (CST; UTC+9:30). As the LAPS forecasts are output three hourly, it is not possible to present the series of cross-sections at the same local time. For this reason, the eastern cross-section begins at 1300 EST (0300 UTC), the northern cross-section at 1230 CST (0300 UTC), and the western cross-section begins at 1400 WST (0600 UTC). The local times are sufficiently close to allow comparison between the cross-sections.

The left columns of Figs 2, 3 and 4 show vertical cross-sections of the mixing-ratio for the eastern, northern and western cross-sections respectively. It is clear from Figs 2, 3 and 4 (left column) that the diffuse mixing-ratio gradient across the continental and tropical air mass boundary dramatically sharpens overnight. The slope of mixing-ratio isopleths, and consequently the dryline, are approximately vertical until the dryline begins to erode after sunrise. The vertical cross-sections suggest that the strongest mixing-ratio gradients occur between the surface and 950 hPa, and are weaker at 925 hPa. However, because the low-level winds are strongest at 950 hPa, the strongest strengthening of the mixing-ratio gradient is expected to occur at 950 hPa rather than at the surface. The lowest levels of the LAPS forecasts are heavily influenced by model boundary-layer parametrisation, and hence care is needed in interpreting moisture at the lowest levels.

Unlike for the Great Plains, Figs 2, 3 and 4 show that after sunrise the nocturnal boundary layer mixes to produce a daytime well-mixed layer of relatively uniform height across the northern Australian continent because the terrain is relatively flat. Consequentially the nocturnal sharp mixing-ratio gradient is eroded through the morning, and is replaced with a broad decrease in moisture toward inland Australia. While the mixing-ratio gradient strengthens from 1300 EST

Fig. 2 Eastern cross-section 1300 EST 13 October–1300 EST 14 October 2002. Left column: mixing-ratio and mixing-ratio gradient. Light shading indicates mixing-ratio gradient greater than $4 \text{ g kg}^{-1} (100 \text{ km})^{-1}$, dark shading indicates greater than $8 \text{ g kg}^{-1} (100 \text{ km})^{-1}$. The contour interval is 1 g kg^{-1} . Centre column: winds parallel to cross-section axis and divergence. The contour interval is 2 m s^{-1} , solid contours are directed inland. Light shading indicates divergence greater than $3 \times 10^{-5} \text{ s}^{-1}$, dark shading indicates convergence greater than $3 \times 10^{-5} \text{ s}^{-1}$. Right column: virtual potential temperature and vertical velocity. The contour interval is 1 K . Shading indicates vertical velocity. The dark-grey shading indicates ascent greater than 0.2 Pa s^{-1} , very dark-grey shading indicates greater than 0.5 Pa s^{-1} . Very light-grey shading indicates descent greater than 0.2 Pa s^{-1} , light grey indicates greater than 0.5 Pa s^{-1} . Vertical axis is pressure (hPa), horizontal axis is kilometres towards coast. Topography is shaded black.

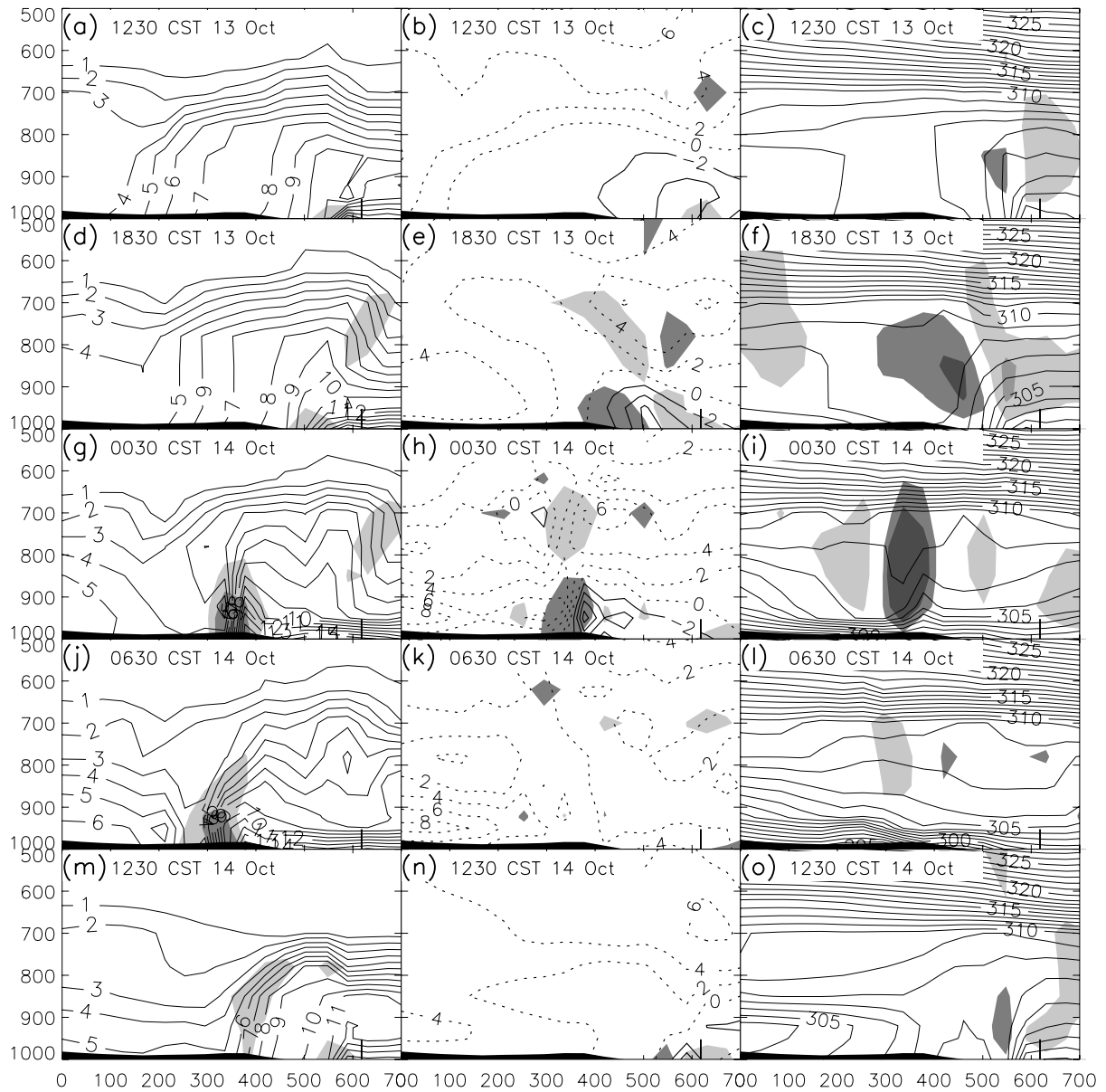


(1230 CST) 13 October to 1300 EST (1230 CST) 14 October in the eastern (northern) cross-section, the diurnal change between day and night is greater than the change from day to day between diurnal cycles. Also, there is very little diurnal movement of the dryline.

In the eastern and northern cross-sections the dryline remains virtually stationary, (Figs 2 and 3: left column), while in the western cross-section (Fig. 4: left column) the region

of maximum mixing-ratio gradient moves gradually inland with the leading edge of the sea-breeze during the afternoon and evening. After 0200 WST, the dryline in the western cross-section tilts toward dry air below 900 hPa, possibly as a result of the toward-trough wind maximum at 900 hPa (Figs 4(g), (h)). In all cases, the location of the dryline is linked to the location of the heat trough, and forms close to the potential temperature maximum.

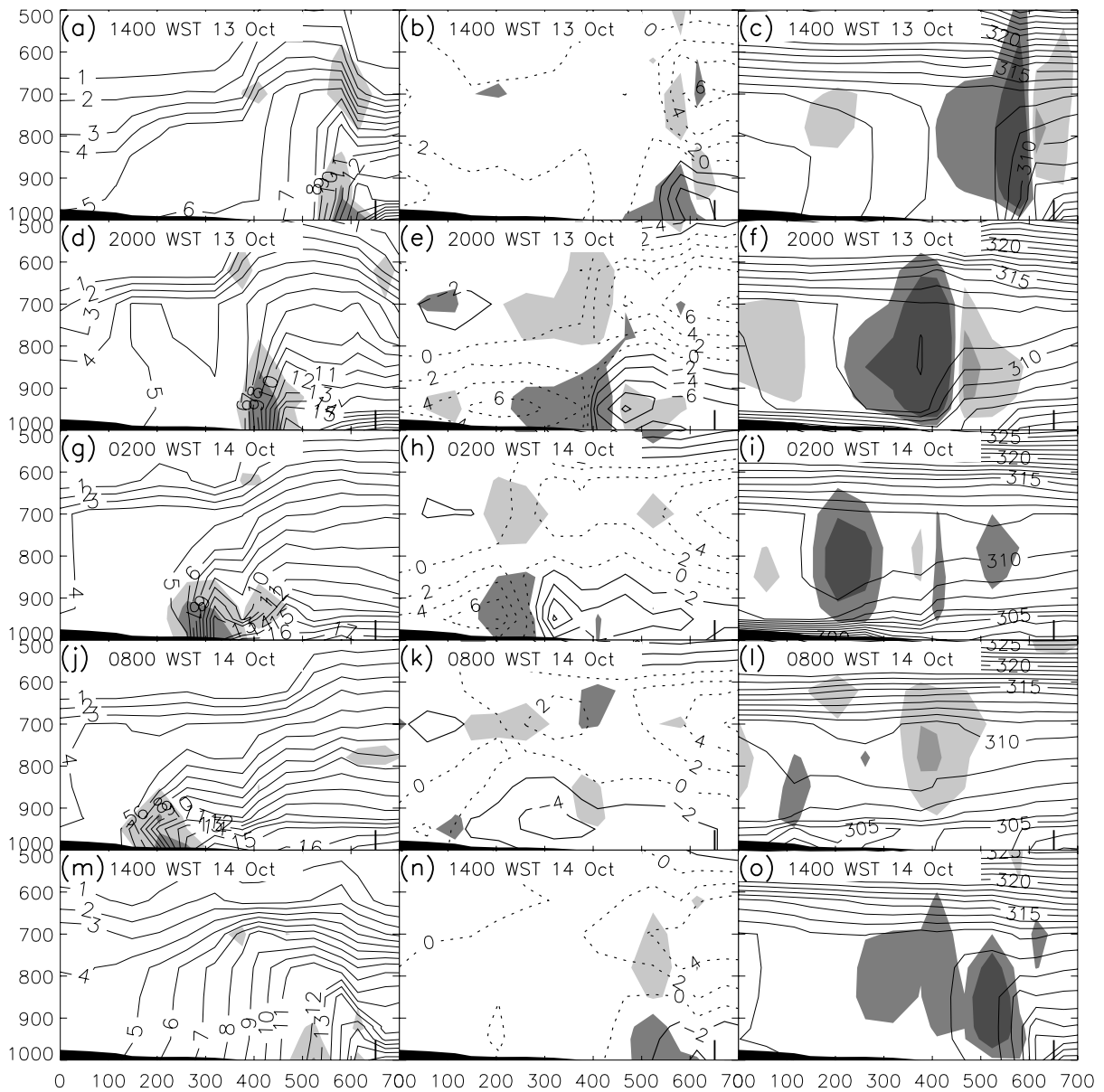
Fig. 3 Northern cross-section 1230 CST 13 October–1230 CST 14 October 2002. Caption as for Fig. 2. The coast is marked by a short solid line.



Virtual potential temperature is defined by $\theta_v = \theta(1+0.61q)$, where θ is the potential temperature and q is the mixing-ratio (kg kg^{-1}). Virtual potential temperature can be used as a surrogate for density, where high virtual potential temperature indicates low density and implies high buoyancy. The right columns of Figs 2, 3 and 4 show the virtual potential temperature across the developing dryline in the eastern, northern and western cross-sections. The virtual potential temperature is almost identical to the potential temperature (not shown), and

hence shows a maximum in the heat trough through the afternoon (Figs 2(c), 3(c) and 4(c); Fig. 1(a)). The moisture content of the air increases towards the coast, increasing the virtual potential temperature. However, the strong decrease in potential temperature toward the ocean dominates the increase in moisture, and as a result there is a strong negative virtual potential temperature gradient towards the coast. The potential temperature maximum within the heat trough leads also to a decrease in virtual potential temperature toward inland Australia.

Fig. 4 Western cross-section 1400 WST 13 October –1400 WST 14 October 2002. Caption as for Fig. 2. The coast is marked by a short solid line.



The density gradients established by the heat trough force a solenoidal circulation in the boundary layer to either side of the trough. The centre columns of Figs 2, 3 and 4 show the component of the wind that is directed toward the heat trough (defined as the component of the wind parallel to the cross-sections in Fig. 1; the positive direction points toward the coast). At low levels these winds are directed toward the heat trough and strengthen through the afternoon as the heat trough deepens. As a consequence, convergence and vertical motion increases within the heat trough also (Figs 2, 3 and 4; centre and right columns).

In the northern and western cross-sections, the sea-breeze circulation is evident by 1830 CST and 1400 WST respectively (Figs 3(d)-(f) and 4(a)-(c)). The ascending branch of

the circulation is located on the coastward edge of the heat trough, and there is divergence and return flow at the top of the boundary layer above the heat trough. The sea-breeze front is marked by strong winds toward the trough, and a relatively sharp mixing-ratio gradient. Behind the sea-breeze front there is upper-level convergence, low-level divergence and subsidence. As the heat trough deepens through the afternoon the sea-breeze circulation strengthens and the sea-breeze front propagates inland.

While the sea-breeze circulation develops also in the eastern cross-section, the ascending branch is not located solely within the heat trough. This is especially evident in the vertical motion and divergence cross-sections (Figs 2(e), (f)), where upward vertical motion and convergence maxima

are located at both the heat trough and the leading edge of the sea-breeze front (Fig. 2(d)). These features suggest two circulations; the sea-breeze circulation, and a second circulation directed toward the heat trough from the inland side. Through the early evening, the sea-breeze circulation advances toward the heat trough, moistening the lower levels of the atmosphere coastward of the heat low.

In the eastern cross-section, elevated terrain lies between the coast and the heat trough, and this may prevent the sea-breeze circulation initially extending to the heat trough as observed in the northern and western cross-sections. However, the heat trough in the eastern cross-section is located further from the coast than in the other two cross-sections (Fig. 1(b)), and this may enable the LAPS forecasts to resolve two separate circulations about the sea-breeze front and heat trough. It is suggested here that in the northern and western cross-sections, two circulations exist initially, but at 0.375° resolution, they appear in the LAPS forecasts as a single circulation.

A weak boundary-layer circulation develops in the dry air inland of the heat trough during the day, and can be seen in all cross-sections by 1900 EST (1830 CST, 2000 WST). There is low-level convergence and upper-level divergence located at the heat trough and return flow and subsidence is evident in the dry air inland of the heat trough. In the eastern cross-section, this circulation is at least as strong as the sea-breeze circulation to the east, leading to the second upward vertical motion and convergence maxima located at the heat trough (Figs 2(e), (f)). Although not as strong as in the eastern cross-section, the western cross-section also shows a second vertical motion and upper-level divergence maxima at the heat trough (Figs 4(e), (f)). In all cross-sections, subsidence in the descending arm of the circulation causes the boundary-layer inland of the heat trough to dry, and at low levels, this increases the moisture gradient across heat trough (Figs 2(d), (f); 3(d), (f) and 4(d), (f)).

After sunset, the boundary-layer circulations on either side of the heat trough dramatically intensify, and continue to strengthen until midnight. It is during this time that the mixing-ratio gradient sharpens into a dryline. Figures 2(i), 3(i) and 4(i) show the development of the nocturnal stable layer at the surface, while Figs 2(h), 3(h) and 4(h) show the consequent nocturnal acceleration of the low-level air toward the heat trough just above the surface. May (1995) has shown that the nocturnal acceleration of the ageostrophic wind toward low pressure is a common feature in the Australian continent. The stratification is stronger in the dry inland air where radiative cooling is more effective and the dry air surges toward the heat trough. This generates strong convergence about the heat trough around midnight (Figs 2(h), 3(h) and 4(h)). The convergence is very pronounced along the northeastern coast when the sea-breeze front accelerates into the heat trough around 2200 EST (Fig. 2(h)). In the western cross-section, the convergence was already strong at 2000 WST because of the pronounced sea-breeze and it weakens slightly by 0200 WST (Figs 4(e), (h)).

Although the convergence maximum occurs near midnight, the mixing-ratio gradient continues to strengthen after midnight while the heat trough weakens overnight. The pressure gradient force remains directed toward the trough. Consequentially the mixing-ratio gradient continues to increase as the winds are accelerated down the pressure gradient, until the turbulent mixing, which develops after sunrise, destroys the stable nocturnal boundary layer. As the Coriolis force turns the winds anticlockwise overnight, an along-dryline jet develops in the dry air (defined as the component of the wind perpendicular to the cross-sections in Fig. 1; the positive direction points into the page; Figs 5 and 1(b)). This is especially conspicuous in the eastern cross-section, where the topography running along the east coast leads to the formation of a barrier jet. Barrier jets are observed frequently in the South Island of New Zealand (Revell et al. 2002), but are not well documented in Australia.

Although not explicitly pointed out by Parker et al. (2005), their Fig. 4 shows that the mixing-ratio gradient across the intertropical convergence zone increases with the nocturnal acceleration of the southwesterly flow over West Africa. The maximum wind speeds occur between 900 and 950 hPa around sunrise. The result is that the mixing-ratio gradient in that study is strongest between 0000 UTC (0000 local time) and 0600 UTC (0600 local time).

Mixing-ratio frontogenesis

Miller (1948) derived an expression for the magnitude of rate of change of the horizontal gradient of a scalar q in a three-dimensional flow. His equation was derived in cartesian coordinates, but can be written more neatly as

$$F_n = - \frac{D}{Dt} |\nabla_h q|$$

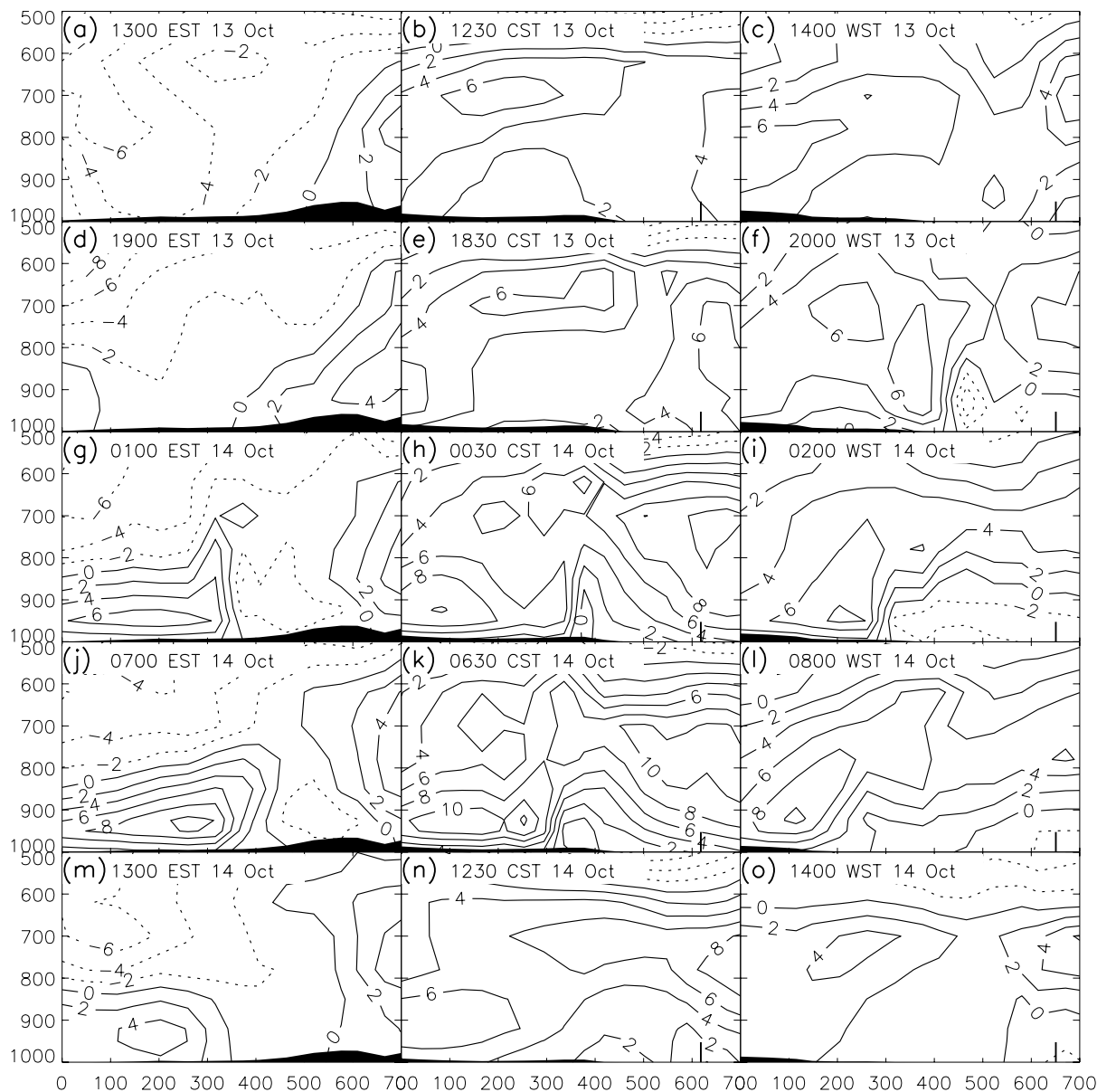
$$= \frac{|\nabla_h q|}{2} D - |\nabla_h q| (E' \cos(2\beta)) - \frac{\partial}{\partial p} (\mathbf{n} \cdot \nabla_h w) + \mathbf{n} \cdot \nabla_h S_q \quad \dots 1$$

where $\mathbf{n} = \nabla_h q / |\nabla_h q|$ is the unit vector pointing along the gradient of q towards lower values; D is the divergence; E' is the total deformation; β is the angle between the axis of dilatation and the isopleths of q ; $w = Dp/Dt$ is the vertical component of velocity, where the vertical coordinate p is pressure; and S_q is the source of q . When q is replaced with mixing-ratio, F_n is the mixing-ratio frontogenesis function.

The terms on the right-hand side of Eqn 1 are referred to as the convergent, deformation, tilting and source mixing-ratio frontogenesis terms respectively. The magnitude of the source term was found to be smaller (not shown) than the convergence and deformation mixing-ratio frontogenesis terms, and consequentially it is omitted from the net mixing-ratio frontogenesis.

The horizontal mixing-ratio frontogenesis, which consists of the convergent and deformation terms in Eqn 1, is shown at 925 hPa in Fig. 6, and corresponds well with the observed

Fig. 5 Winds perpendicular to cross-section axis. Left column: eastern cross-section. Centre column: northern cross-section. Right column: western cross-section. The contour interval is 2 m s^{-1} , solid contours are directed into the page. Vertical axis is pressure (hPa), horizontal axis is kilometres towards coast. Topography is shaded black. The coast is marked by a short solid line.



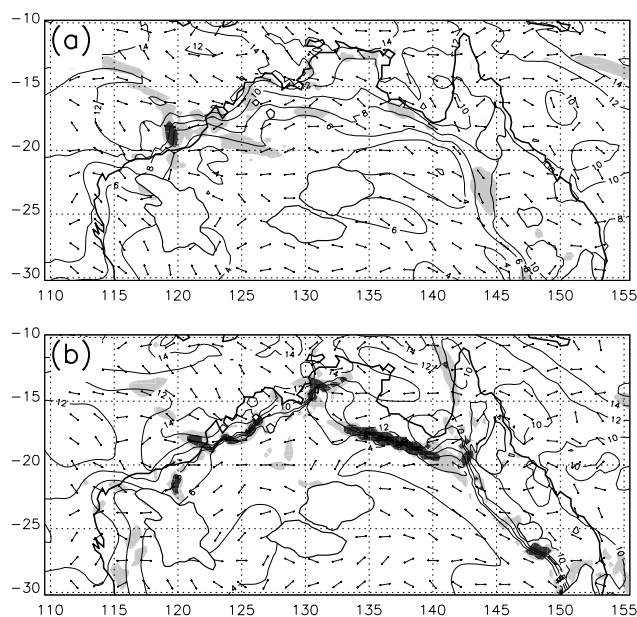
development of the dryline in Fig. 1. The cross-sections of mixing-ratio frontogenesis including the tilting term are presented in Figs 7, 8 and 9 (left column). The maxima of the convergent and deformation terms occur around 950 hPa, where the low-level winds are strongest.

At low levels, the convergent term (centre column) and deformation term (right column) in the mixing-ratio frontogenesis function explain the development and evolution of the mixing-ratio gradient; the contribution by the tilting term is small as $\partial q/\partial p$ is small in the boundary layer. However, above around 900 hPa, mixing-ratio frontogenesis is dominated by the tilting term. At these levels there is strong

vertical motion as a result of the low-level convergence, which in turn leads to vertical tilting of the mixing-ratio isopleths and an increase in the upper-level mixing-ratio gradient overnight. Thus, the tilting term appears important for the observed overnight strengthening of the mixing-ratio gradient between 900 and 700 hPa. Nonetheless, the mixing-ratio gradient at this height remains much weaker than at low levels.

The eastern, northern and western vertical cross-sections show that strong convergence develops overnight where there is a nocturnal acceleration of air toward the heat trough. Since convergence always acts to increase the mix-

Fig. 6 Mixing-ratio frontogenesis function and axis of dilatation at 925 hPa. Light shading indicates mixing-ratio frontogenesis rate $2 \times 10^{-5} \text{ g kg}^{-1}(100 \text{ km})^{-1}\text{s}^{-1}$, dark shading indicates mixing-ratio frontogenesis rate greater than $10 \times 10^{-5} \text{ g kg}^{-1}(100 \text{ km})^{-1}\text{s}^{-1}$. (a) 1300 EST (1100 WST) 13 October 2002. (b) 0100 EST (2300 WST) 14 (13) October 2002. The ordinate is longitude in degrees and the abscissa is latitude in degrees. The blank areas enclosed with solid dark lines indicate topography above 500 m



ing-ratio gradient, convergent mixing-ratio frontogenesis develops in the heat trough and reaches a maximum when the convergence and nocturnal acceleration of the dry inland and moist coastal air mass is strongest. This maximum occurs around 0100 EST (0030 CST) in the eastern and northern cross-sections (Figs 7(h) and 8(h)).

Along the northwestern coast the strongest acceleration of the coastal air mass toward the heat trough occurs several hours before the nocturnal acceleration of the inland air mass reaches a maximum (Figs 4(e), (h)). This is because the heat trough is especially deep over northwestern Australia leading to a strong sea-breeze circulation during the afternoon (Fig. 1(a)). In contrast to the eastern and northern cross-sections the inland acceleration of the coastal air mass decreases after 2000 WST when the heat trough weakens. As a result, in the western cross-section the maximum convergent mixing-ratio frontogenesis occurs at 2000 WST when convergence is strongest (Fig. 9(e)). Despite the subsequent weakening of the inland acceleration of the coastal air mass between 2000 WST and 0200 WST, the nocturnal acceleration of the dry air strengthens, and hence convergence remains strong and considerable convergent mixing-ratio frontogenesis persists overnight (Fig. 9(h)) leading to the observed increase in the mixing-ratio gradient over that time.

In all cross-sections, the convergent mixing-ratio frontogenesis maxima extend to 850 hPa, and above this height, the convergent term is frontolytic because of upper-level divergence (Figs 7, 8 and 9; centre column). Although the maximum convergent mixing-ratio frontogenesis occurs at around midnight, when convergence is strongest, it persists until sunrise and causes the mixing-ratio gradient to continue to strengthen overnight.

Deformation is strong also about the heat trough and sea-breeze fronts at low-levels, however it leads only to mixing-ratio frontogenesis when the angle between the axis of dilatation and mixing-ratio isopleths is less than 45° ($|\nabla_h q| (E' \cos(2\beta)) > 0$; Figs 7, 8 and 9; right column). This occurs poleward of the Gulf of Carpentaria. Mixing-ratio frontogenesis is weaker elsewhere along the heat trough because deformation is frontolytic in many regions, especially along the northeastern coast (Fig. 6(b)).

The northern cross-section, taken poleward of the Gulf of Carpentaria, shows that the contribution to mixing-ratio frontogenesis by deformation becomes large by 0030 CST (Fig. 8(i)) and reaches a maximum at 0330 CST, before sunrise (not shown). The deformation mixing-ratio frontogenesis maximum is as large as the convergent mixing-ratio frontogenesis maximum, which occurred some hours earlier. The deformation mixing-ratio frontogenesis maximum strengthens as the nocturnal ageostrophic winds rotate overnight and the axis of dilatation becomes aligned with the heat trough before sunrise.

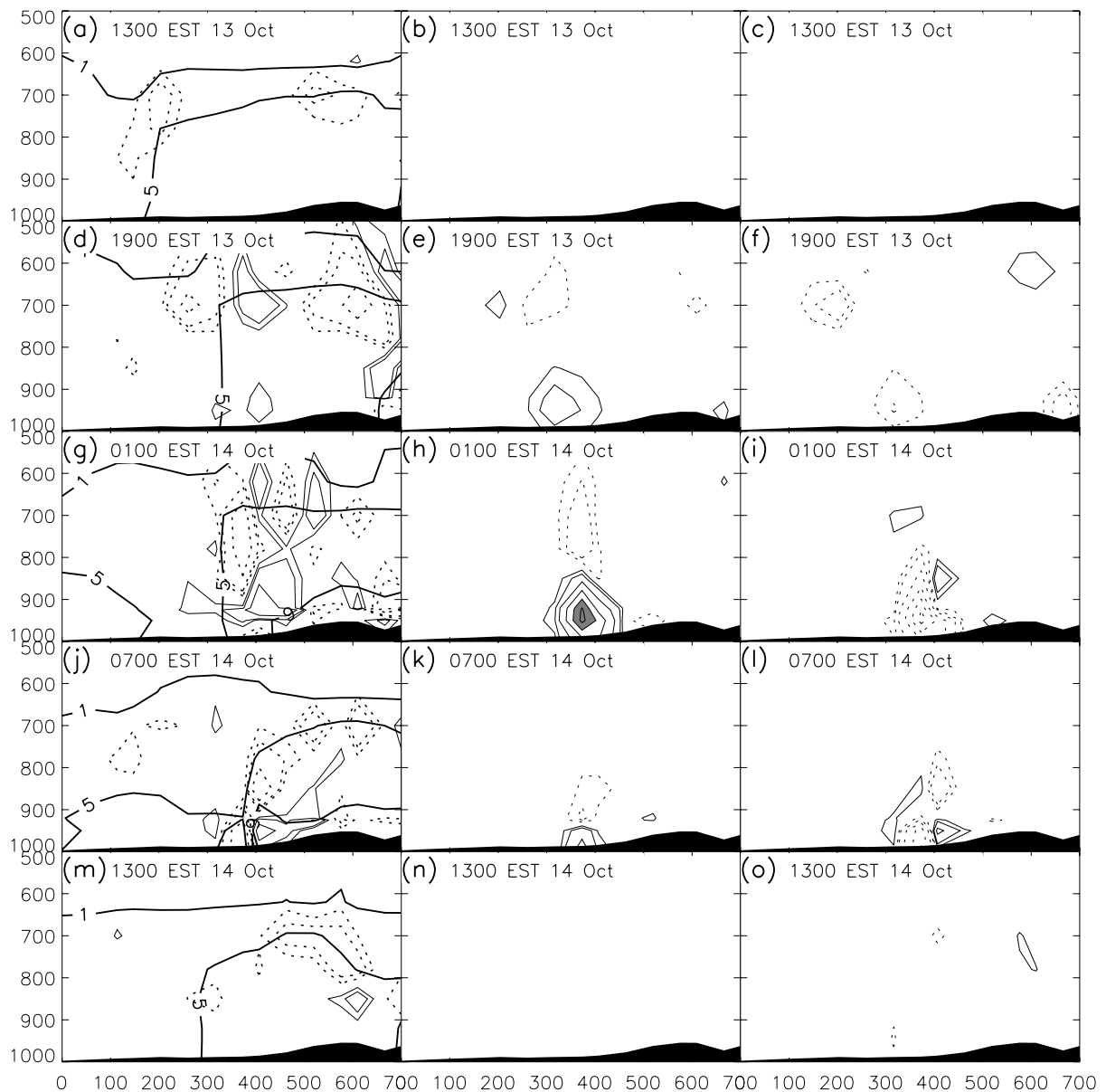
The contribution to mixing-ratio frontogenesis by deformation in the western cross-section follows a similar evolution to the northern cross-section. Deformation mixing-ratio frontogenesis is largest before sunrise at 0200 WST, and is larger than the convergent mixing-ratio frontogenesis at 2000 WST. In the western cross-section deformation mixing-ratio frontogenesis becomes large by 2000 WST when the sea-breeze is strong (Fig. 9(f)).

In contrast, the eastern cross-section shows that deformation leads to mixing-ratio frontolysis. This is especially pronounced at 0030 CST when the deformation is strongest (Fig. 7(i)). As a result, the rate of the strengthening of the dryline depends on the sign and relative magnitude of the convergent and deformation terms in Eqn 1. However, Fig. 6 shows that the net effect is mixing-ratio frontogenesis throughout the night along much of the northeastern coast, producing the sustained nocturnal strengthening of the dryline observed across northern Australia in Fig. 1.

A comparison of the LAPS forecasts with observational data

There are a number of data sources available that can be used to verify the development of the air mass boundaries over northern Australia forecast by LAPS. These data include the AWS observations, radiosonde observations and AIRS satellite data.

Fig. 7 Eastern cross-section 1300 EST 13 October–1300 EST 14 October 2002. Left column: mixing-ratio frontogenesis and mixing-ratio. The solid contours indicate mixing-ratio frontogenesis, and the dotted contours indicate mixing-ratio frontolysis. The contour intervals have magnitude 50, 100, 250 $\times 10^{-5} \text{ g kg}^{-1}(100 \text{ km})^{-1}\text{s}^{-1}$ then increase by 250 $\times 10^{-5} \text{ g kg}^{-1}(100 \text{ km})^{-1}\text{s}^{-1}$. Dark shading indicates mixing-ratio frontogenesis greater than 750 $\times 10^{-5} \text{ g kg}^{-1}(100 \text{ km})^{-1}\text{s}^{-1}$. The thick solid lines show selected mixing-ratio contours (g kg^{-1}). Centre column: mixing-ratio frontogenesis function convergent term. The contour intervals and shading are as for the left column. Right column: mixing-ratio frontogenesis function deformation term. The contour intervals and shading are as for the left column. Vertical axis is pressure (hPa), horizontal axis is kilometres towards coast. Topography is shaded black.



The combined AWS and manual remote outstation observations provide three-hourly dew-point (which have been converted to mixing-ratio in this paper for comparison), temperature, pressure and wind data. The AWS and manual observations only include data that have been quality controlled, and therefore represent the most accurate observational data of the environment for comparison with the LAPS forecasts. However, the observational network is relatively sparse and irregular and confined to the sur-

face. As a result, it is difficult to quantify the diurnal cycle of the mixing-ratio gradient in the AWS and manual observations. Furthermore, because the dryline is relatively stationary and there are large distances between AWS, the mixing-ratio gradient frequently strengthens into a dryline between AWS locations. Despite these limitations, the AWS and manual observations presented in this section show strong evidence for the nocturnal strengthening of the mixing-ratio gradient.

Fig. 8 Northern cross-section 1230 CST 13 October–1230 CST 14 October 2002. Caption as for Fig. 7. The coast is marked by a short solid line.

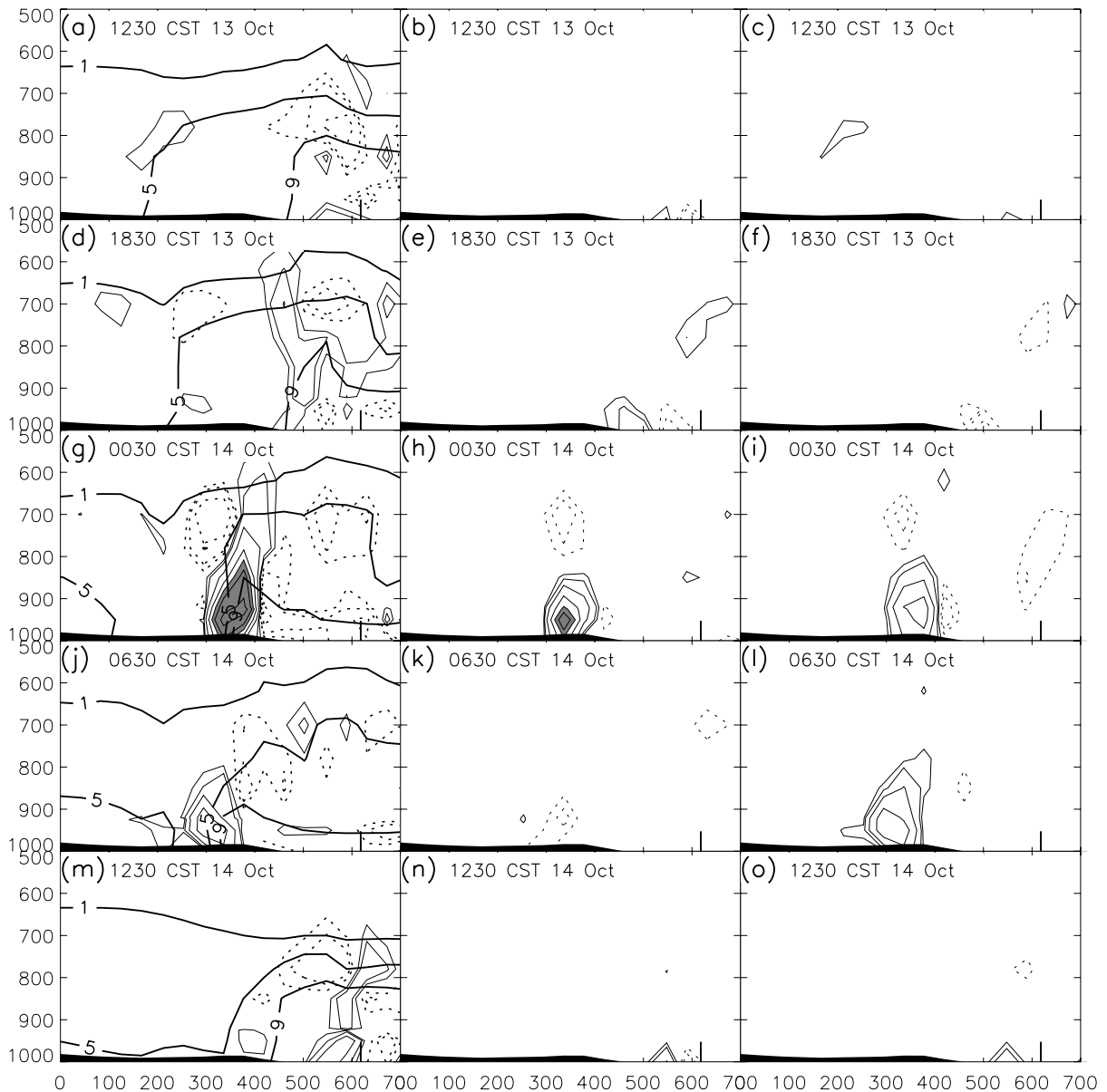


Figure 10 compares the radiosonde observations and AWS surface observations at Mt Isa with the closest LAPS forecast model point to Mt Isa from 1600 EST 13 October to 1000 EST 14 October 2002. The left panel in Fig. 10 shows the development of the nocturnal jet between 950 – 900 hPa in both the radiosonde observations (solid lines) and the LAPS forecasts (dashed lines). Because of this, the strongest mixing-ratio gradients are expected to develop around 950 hPa. Indeed, this is the height where the strongest mixing-ratio frontogenesis is observed in

the LAPS forecasts (Figs 7, 8 and 9). Since the AWS and manual observations (squares in Fig. 10) are recorded below the height of the nocturnal jet, the maximum strength of the mixing-ratio gradient is not captured in these observations. Consequently, the passage of a dryline through an individual AWS may not show a pronounced signature. Nonetheless, the network of AWS and manual observations reveal the large-scale rearrangement of the low-level environment that produces the strengthening of the low-level moisture gradient into a dryline.

Fig. 9 Western cross-section 1400 WST 13 October–1400 WST 14 October 2002. Caption as for Fig. 7. The coast is marked by a short solid line.

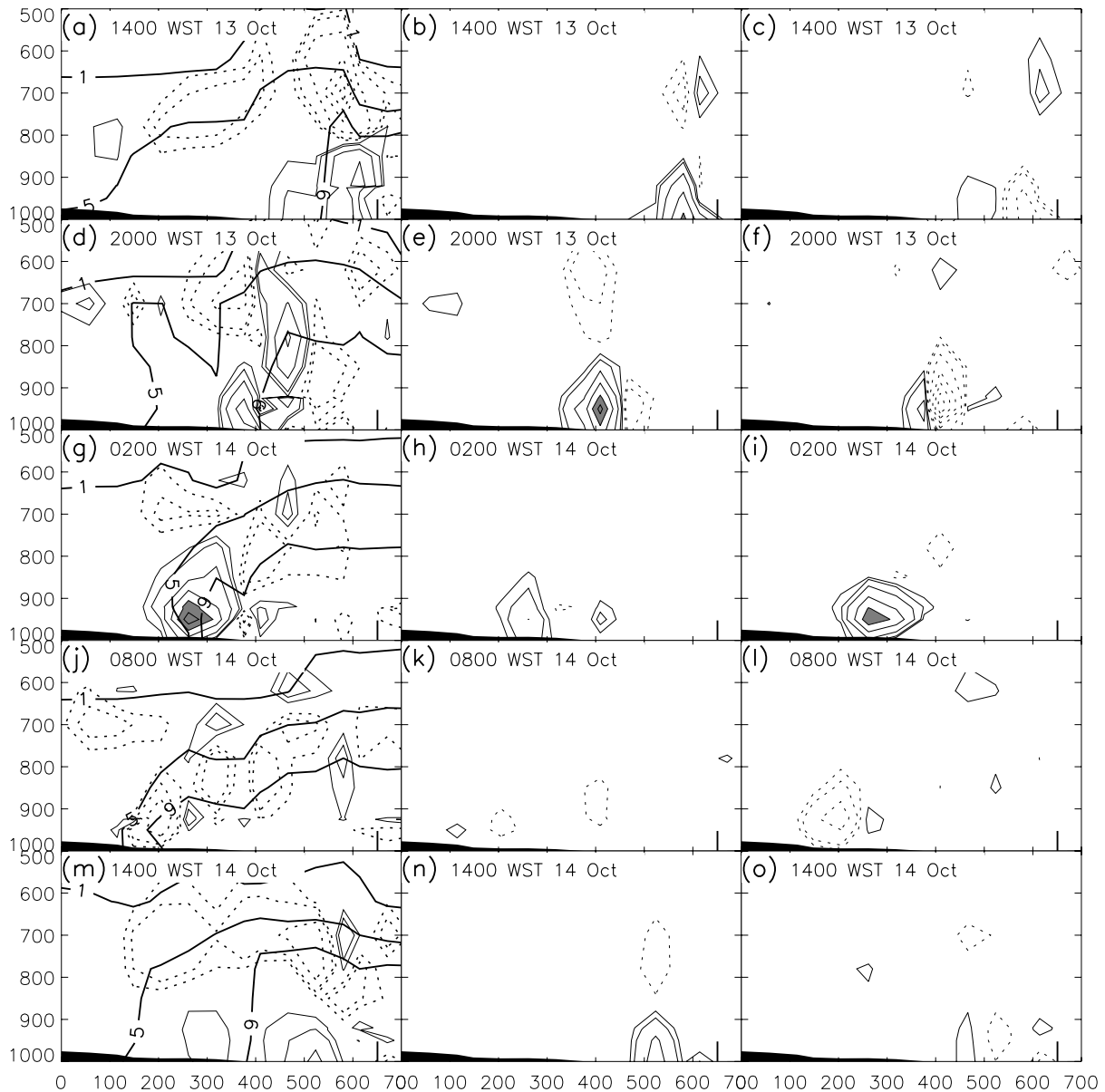


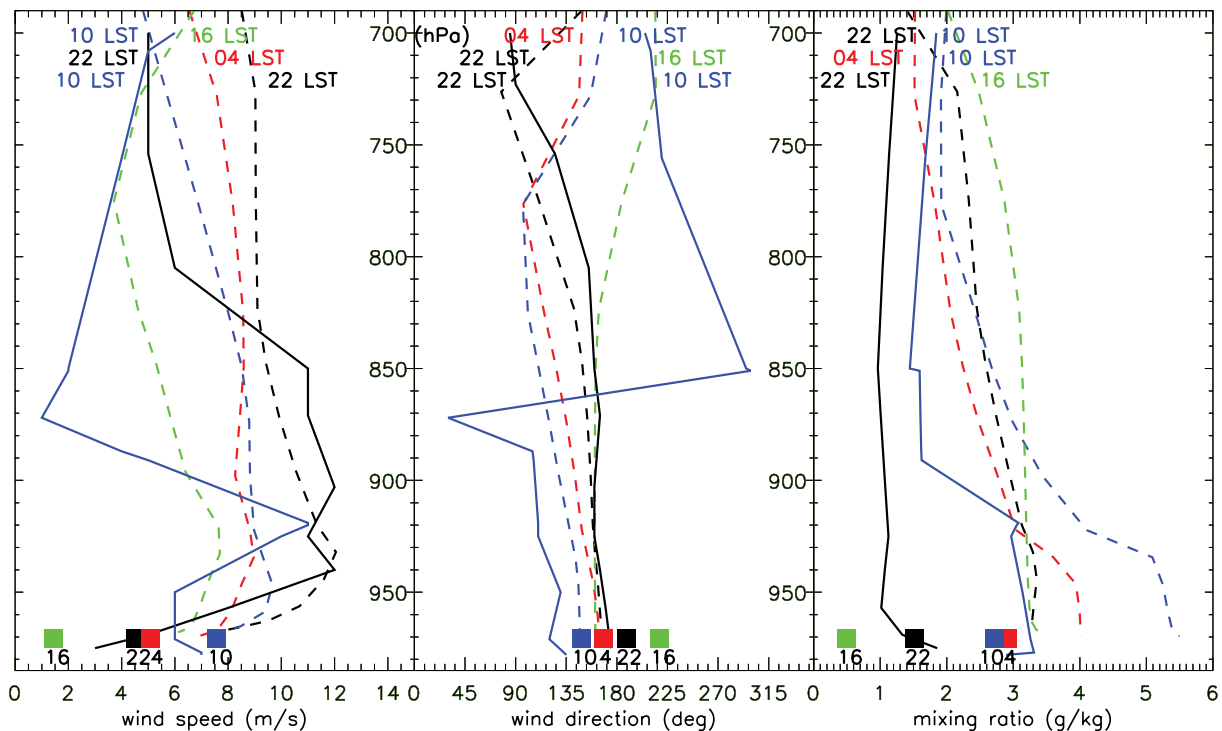
Figure 11 shows 48-hour time series from 0000 EST 14 October to 2359 EST 16 October of AWS observations from Burketown and Cloncurry, which are located either side of the dryline, (see Fig. 1(d) for locations of AWSs). The triangles mark the LAPS forecast of the screen height temperatures and 10 m height winds.

At Burketown (Fig. 11(a)), the trace shows the development of moist onshore northerly flow shortly after sunrise on 14 October, which gradually rotates anticlockwise after sunset (1900 EST). At sunrise (0700 EST) on 15 October there is a sudden drop in dew-point of 16°C and an increase in the wind speed, which corresponds to the arrival of south-

erly flow. This change marks the passage of the dryline. The passage of the dryline is clear in the LAPS forecast also and shows the same magnitude of change as the AWS observations, but is around four hours too early. As there are a very limited number of AWS observations that record the passage of a dryline, it is not clear whether this is typical. On this day, the LAPS forecast shows excellent agreement with the wind direction and temperature, but produces some differences in the wind speed.

At Cloncurry (Fig. 11(b)) the wind direction remains southerly and the environment is dry throughout the 48-hour period. The wind field and temperature show excellent

Fig. 10 Comparison between LAPS three-hour forecast, AWS observations and upper-air sounding at Mount Isa from 1600 LST 13 October 2002–1000 LST 14 October 2002. Dashed lines indicate LAPS three-hour forecast, solid lines indicate upper-air sounding, and solid squares indicate AWS observations. Numbers under the solid squares indicate Local Standard Time. Left: wind speed (m s^{-1}). Centre: wind direction where 0 indicates winds from the north. Right: mixing-ratio (g kg^{-1}).



agreement with the LAPS forecast, while the dew-point is consistently too high. The change from the LAPS 24-hour forecast for 14 October to the 24-hour forecast for 15 October at 0000 EST 14 October produces a sharp jump in the dew-point, and shows the tendency of LAPS to moisten the surface over time.

The network of AWS and manual observations are compared with the lowest sigma level ($\sigma = 0.9988$) of the LAPS forecasts in Fig. 12 which is approximately 10 metres above the surface. A strong coastal temperature gradient is evident in the AWS and manual observations during the day, Figs 12(a), (b) showing the resultant coastal moisture gradient and sea-breeze circulation. The development of the sea-breeze is not fully captured in the LAPS three-hour forecast, however the winds are generally onshore around the coast and there is a sharp moisture gradient. Across the northwestern coastline there is a mixing-ratio change of up to 7 g kg^{-1} .

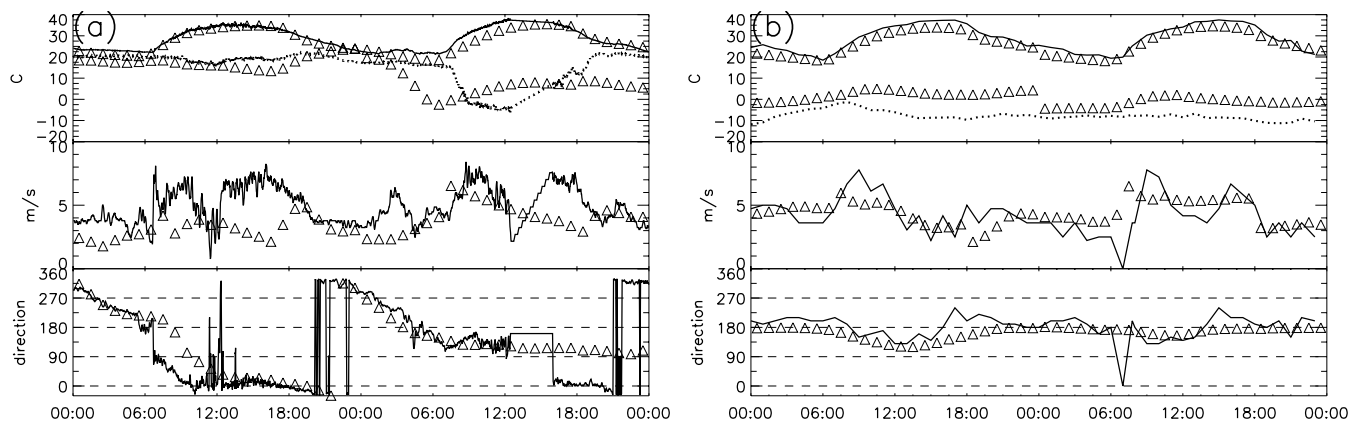
The AWS and manual observation of the winds and the LAPS three-hour forecasts show excellent agreement inland. Overnight, both sets of data show an anticlockwise inertial turning of the winds (Fig. 12(f)). Low values of mixing-ratio are observed inland of the dryline, and high values of mixing-ratio toward the coast (Fig. 12(e)). The mixing-ratio field in the AWS and manual observations show also that the moist northern air moves inland in agreement with the

LAPS three-hour forecasts. However, the LAPS three-hour forecasts appear to underestimate the moisture content of the offshore air mass and overestimate the inland moisture content. This is seen also in Fig. 10 (right panel) at Mt Isa, which is inland of the dryline. Although the LAPS forecasts overestimate the moisture content at Mt Isa, the relative difference in moisture between day and night is similar in the LAPS forecasts and the observations.

During the period 13 – 14 October 2002, mixing-ratios are available over Australia from AIRS (NASA 2008; see Data section). Figures 12(c), (d), (g) and (h) show a comparison between the LAPS three-hour forecasts and the AIRS satellite data at 1600 EST (1400 WST) 13 October and 0400 EST (0200 WST) 14 October. The air mass boundary that gives rise to the dryline is clearly visible in the satellite images and is in the same location as forecast by LAPS. Although there are differences in the magnitude of the low-level moisture between AIRS and the LAPS forecasts, the AIRS data show excellent agreement with the relative diurnal changes in low-level moisture forecast by LAPS.

During the day, the strong coastal moisture gradient, which develops as a result of the sea-breeze circulation, is evident to the north and west of Australia in the AIRS images in Fig. 12(d). At this time, the inland air mass is up to 5 g kg^{-1} drier in the AIRS data (Fig. 12(d)) than in the LAPS

Fig. 11 AWS observations and LAPS surface forecasts from 0000 LST 14 October–2359 LST 15 October 2002 for (a) Burketown: GLEX one-minute AWS, LAPS surface forecast (triangles). (b) Cloncurry: Bureau of Meteorology one-hour AWS observations and LAPS surface forecast (triangles). For each figure, top panel: temperature (solid line); dew-point (dashed line). Middle panel: wind speed. Bottom panel: direction of wind origin.



three-hour forecasts (Fig. 12 (c)). This is consistent with AWS and manual observations (Fig. 12(a)) and further suggests that the LAPS forecast may overestimate inland moisture near the surface.

The AIRS satellite images show a large change in moisture between day (Fig. 12(d)) and night (Fig. 12(h)) of up to 5 g kg^{-1} over inland northern Australia. While the spatial pattern of this change is in good agreement with the LAPS forecasts, the magnitude of the inland moistening seems unrealistic and is not supported by the AWS and manual observations. As a result, AIRS may underestimate the difference in moisture between the dry continental and moist tropical air mass overnight.

Although there are some differences between AIRS, the AWS and manual observations and the LAPS forecasts, the AIRS data show clearly the development of a sharp moisture gradient across the heat trough overnight as the moist tropical air mass moves inland. The location of this sharp moisture gradient is in excellent agreement with the position of the convergence line in the nocturnal wind field found in both the LAPS three-hour forecast and the AWS and manual observations which marks the dryline (Fig. 12(f)).

Discussion

The mechanisms which strengthen the Australian dryline are different to those which act on the Great Plains dryline, and consequentially the diurnal cycles are different. A schematic comparison of the development of the Great Plains and the northern Australian dryline is shown in Fig. 13.

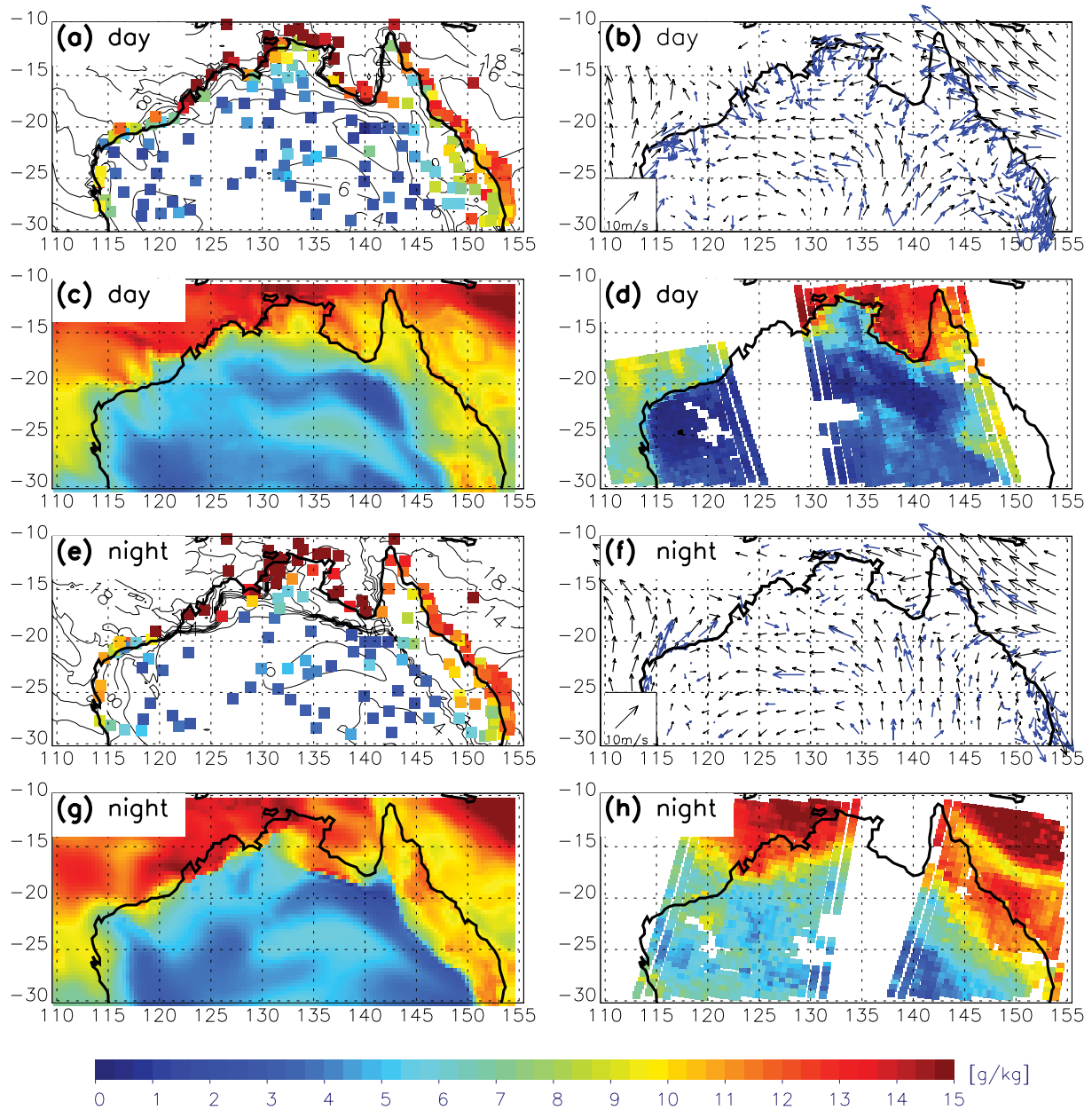
Over the Great Plains, deepening of the lee trough to the east of the Rocky Mountains leads to large-scale confluence between moist and dry air and creates a favourable environment for the development of strong drylines (Schultz et

al. 2007). On the smaller scale, vertical mixing of heat and momentum across the top of the convective boundary layer and mixing-ratio frontogenesis sharpen the diffuse moisture gradient into a dryline.

The terrain of the Great Plains slopes downward to the east, and as a result the depth of the moist nocturnal boundary layer increases also towards the east. In comparison, the terrain over northern Australia is relatively flat and a diffuse moisture gradient remains centred on the heat trough that develops during the day.

During the day, surface heating leads to the development of a heat trough over both the Great Plains and northern Australia. On the moist side of both the northern Australian and Great Plains drylines, the decrease in density toward the heat trough forces a solenoidal boundary-layer circulation in the afternoon. This drives the sea-breeze circulation in Australia and what Sun and Ogura (1979) termed the 'inland sea breeze' over the Great Plains. On the dry side of the dryline, the downward transfer of momentum over the Great Plains increases the westerly surface winds, especially when a strong mid-level westerly jet overspreads the dryline. This vertical transport of westerly momentum is an essential mechanism for the sharpening of the Great Plains dryline (Schultz et al. 2007). The westerly winds oppose the low-level easterlies in the moist air and lead to convergent mixing-ratio frontogenesis (Sun and Wu 1992; Ziegler et al. 1995). As a consequence, the Great Plains mixing-ratio gradient is strongest during the afternoon when turbulent mixing is strongest. In contrast, the topography of northern Australia is relatively flat, and as a result there is no differential downward mixing of momentum across the dryline, as seen in Figs 2 to 4(b), (c). However, because the Australian dryline is centred over the heat trough, a solenoidal circulation also develops in the dry air inland. The low-level flow and inland subsidence associated with this circulation act to further increase the moisture gradient across the heat trough.

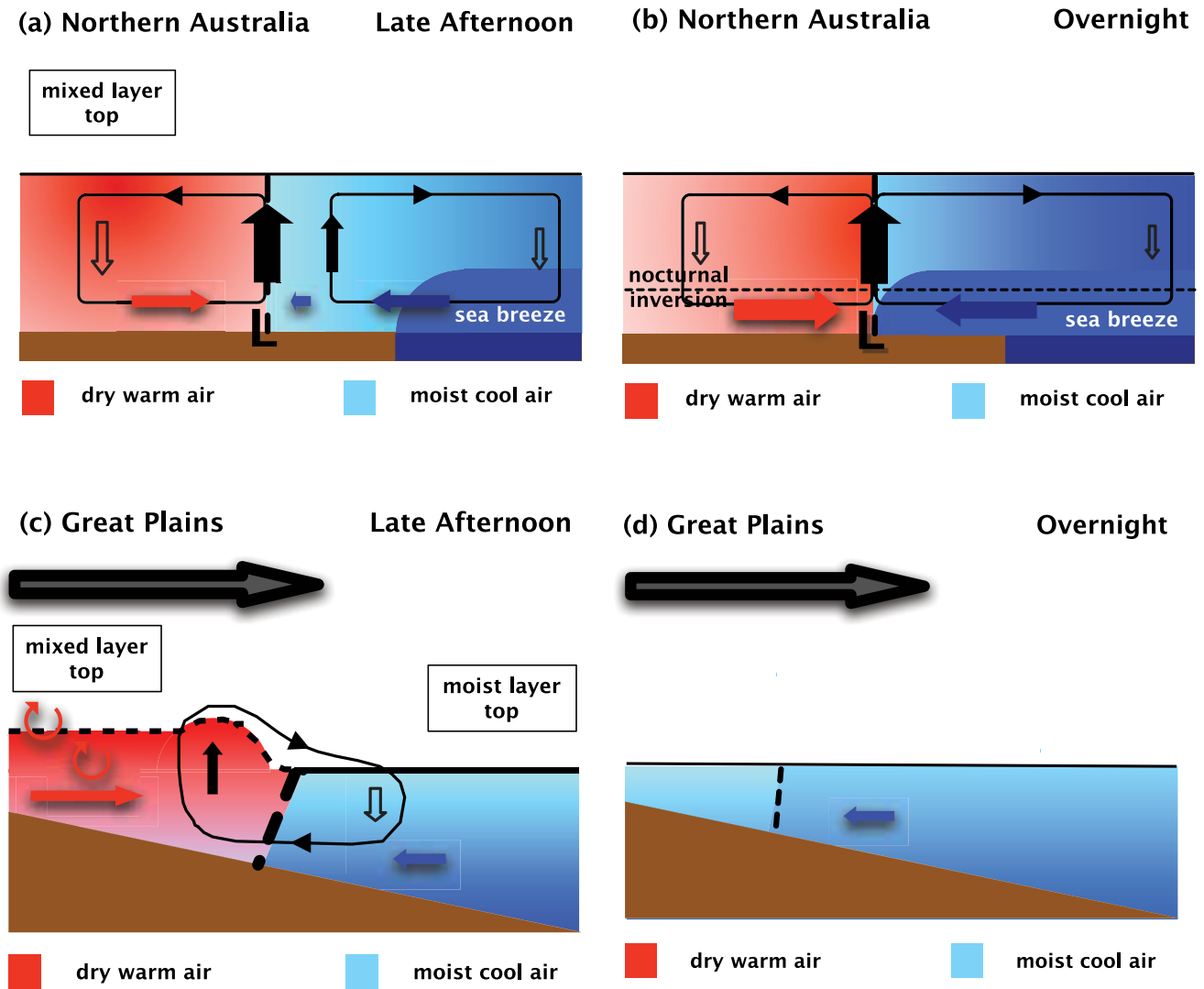
Fig. 12 Comparison between LAPS three-hour forecast, AWS observations and AIRS satellite data. (a) Mixing-ratio for LAPS three-hour forecasts at $\sigma = 0.9988$ (contours) and the AWS and manual observations at 10 m (filled boxes). The contour interval is 1 g kg^{-1} . LAPS three-hour forecast at 1600 EST (1400 WST) 13 October 2002 and AWS observations at 1500 LST. (b) Winds for LAPS three-hour forecasts at $\sigma = 0.9988$ (black arrows) and the AWS and manual observations at 10 m (blue arrows). LAPS three-hour forecast at 1600 EST (1400 WST) 13 October 2002 and AWS and manual observations at 1500 LST. (c) LAPS three-hour forecast at 925 hPa, 1600 EST (1400 WST) 13 October 2002. (d) AIRS at 1000 hPa, 1430–1606 EST (1230–1406 WST) 13 October 2002. (e) Mixing-ratio for LAPS three-hour forecasts at $\sigma = 0.9988$ (contours) and the AWS and manual observations at 10 m (filled boxes). The contour interval is 1 g kg^{-1} . LAPS three-hour forecast at 0400 EST (0200 WST) 14 October 2002 and AWS observations at 0300 LST. (f) Winds for LAPS three-hour forecasts at $\sigma = 0.9988$ (black arrows) and the AWS and manual observations at 10 m (blue arrows). LAPS three-hour forecast at 0400 EST (0200 WST) 14 October 2002 and AWS and manual observations at 0300 LST. (g) LAPS three-hour forecast at 925 hPa, 0400 EST (0200 WST) 14 October 2002. (h) AIRS at 1000 hPa, 0130–0306 EST (2330–0106 WST) 14 October 2002.



At dusk surface heating wanes and the effect of surface friction on the flow above is reduced. The boundary layer stratifies, the mixed-layer depth reduces and a nocturnal temperature inversion forms. The surface layer decouples from the layer above the temperature inversion. As a result of these

processes, the Australian dryline continues to strengthen overnight above the surface, while the Great Plains dryline reaches a maximum in the late afternoon before decaying and retreating westward. Nocturnal cooling suppresses the downward transport of westerly momentum over the Great

Fig. 13 Schematic showing the development of the northern Australian and Great Plains dryline. Arrows indicate air flow direction. Long arrow denotes synoptic westerlies above the mixed layer. Circular arrows indicate mixing and entrainment of upper-level dry air. Colour indicates moisture: dark red – very dry; to dark blue – very moist. Dashed line marks the location of the dryline.



Plains and it follows that convergence at the dryline weakens. The moist easterly winds surge forward toward the location of the daytime heat trough until the pressure gradient across the dryline reverses after midnight (Sun and Wu 1992; Ziegler et al. 1995). With time, the Coriolis deflection of the ageostrophic easterly wind generates a low-level southerly jet in the moist air (Ziegler and Hane 1993; Miller et al. 2001; Jones and Bannon 2002). Meanwhile, horizontal mixing across the dryline in the early hours of the morning causes the moisture gradient to weaken and the dryline becomes ill-defined (Miller et al. 2001; Schaefer 1986).

In contrast, the Australian dryline remains within the heat trough throughout the night. Air surges toward the heat trough from both sides of the dryline, especially from

the dry continental inland, where nocturnal cooling is strongest. The pressure gradient does not reverse overnight, and convergence continues until the surface heating and the associated mixing decelerates the low-level flow. In addition, Coriolis deflection of the winds leads to a favourable alignment between the axis of dilatation and dryline before sunrise along the western and northern coastlines. As a result, the Australian dryline strengthens until sunrise.

Conclusions

Across northern Australia, the dryline is a major feature of the low-level atmospheric environment. The dryline forms above the surface as a result of the diurnally varying circula-

tion about the heat trough which extends east-west across northern Australia. During the day a sea-breeze circulation develops about the coast, and overnight there is a nocturnal acceleration of both the dry inland air mass and the moist coastal air mass toward the heat trough. This leads to the nocturnal strengthening of the moisture gradient across the air mass boundary between the inland dry air mass and the tropical moist air mass into a dryline.

The development of the dryline can be described in terms of mixing-ratio frontogenesis. At low levels the dominant terms in the mixing-ratio frontogenesis equation are the convergent and deformation terms. Since convergence always acts to increase the mixing-ratio gradient, convergent mixing-ratio frontogenesis develops in the heat trough and reaches a maximum when the acceleration of the dry inland and moist coastal air mass is strongest. This occurs between the early evening and midnight. Along the northwestern coast the sea-breeze is especially strong, and convergent mixing-ratio frontogenesis peaks in the early evening when the sea-breeze is strongest but remains large through to midnight as the acceleration of the inland air mass toward the heat trough develops. The deformation mixing-ratio frontogenesis strengthens after the convergent mixing-ratio frontogenesis and reaches a maximum before sunrise as the nocturnal ageostrophic winds rotate overnight and the axis of dilatation becomes aligned with the heat trough. However, deformation only leads to mixing-ratio frontogenesis when the angle between the axis of dilatation and mixing-ratio isopleths is less than 45° . Along the northeastern coast, the angle between the axis of dilatation and mixing-ratio isopleths is frequently greater than 45° , leading to localised regions of mixing-ratio frontolysis despite overall mixing-ratio frontogenesis. As a result, the rate of the strengthening of the dryline depends on the sign and relative magnitude of the convergent and deformation terms.

The effect of the diurnal cycle on the northern Australian environment extends well beyond the development of a dryline, suggesting two extensions to the work presented here. First, it is likely that the nocturnal acceleration of moist air toward the heat trough is an important moisture source in the northern Australian environment, and warrants further investigation. Second, preliminary analyses show that nocturnal convergence into the heat low coincides with a peak in convection in the early hours of the morning over northwestern Australia. Clearly, the diurnally varying circulation plays a central role in much of the meteorology over northern Australia.

Acknowledgments

We would like to thank Blair Trewin (Centre for Australian Weather and Climate Research) for providing AWS data, and Roger Smith (Meteorological Institute, University of Munich) for providing AWS data for the time series from Burketown. We are grateful to Graham Mills (Centre for Australian Weather and Climate Research) for his detailed review.

References

- Adams, M. 1993. A linear study of the effects of heating and orography on easterly airstreams with particular reference to northern Australia. *Aust. Met. Mag.*, 42, 69–80.
- Arnup, S.J. and Reeder, M.J. 2007. The diurnal and seasonal variation of the northern Australian dryline. *Mon. Weath. Rev.*, 135, 2995–3008.
- Fandry, C.B. and Leslie, L.M. 1984. A two-layer quasi-geostrophic model of summer trough formation in the Australian subtropical easterlies. *J. Atmos. Sci.*, 41, 807–18.
- Goler, R., Smith, R.K., Reeder, M.J., Arnup, S.J., Richter, H., Keenan, T., May, P. and Hacker, J. 2006. Low-level convergence lines over north-eastern Australia. Part I: the north Australian cloudline. *Mon. Weath. Rev.*, 134, 3092–108.
- Jones, P.A. and Bannon, P.R. 2002. A mixed-layer model of the diurnal dryline. *J. Atmos. Sci.*, 59, 2582–93.
- Kepert, J.D. and Smith, R.K. 1992. A simple model of the Australian west coast trough. *Mon. Weath. Rev.*, 120, 2042–55.
- Keyser, D., Reeder, M.J. and Reed, R.J. 1988. A generalization of Pettersen's frontogenesis function and its relation to vertical motion. *Mon. Weath. Rev.*, 116, 762–80.
- May, P.T. 1995. The Australian nocturnal jet and diurnal variations of the boundary layer winds over Mt Isa in northeastern Australia. *Q. Jl R. Met. Soc.*, 121, 987–1003.
- Miller, J.A., Kovacs, T.A. and Bannon, P.R. 2001. A shallow-water model of the diurnal dryline. *J. Atmos. Sci.*, 58, 3508–24.
- Miller, J.E. 1948. On the concept of frontogenesis. *J. Atmos. Sci.*, 5, 169–71.
- National Aeronautics and Space Administration, Cited 2008. AIRS Data. <http://disc.gsfc.nasa.gov/AIRS/documentation>.
- Parker, D.J., Burton, R.R., Diongue-Niang, A., Ellis, R.J., Felton, M., Taylor, C.M., Thorncroft, C.D., Bessemoulin, P. and Tompkins, A.M. 2005. The diurnal cycle of the West African monsoon circulation. *Q. Jl R. Met. Soc.*, 131, 2839–60.
- Puri, K., Dietachmayer, G.S., Mills, G.A., Davidson, N.E., Bowen, R.A. and Logan, L. W. 1998. The new BMRC Limited Area Prediction System, LAPS. *Aust. Met. Mag.*, 47, 203–23.
- Revell, M.J., Copeland, J.H., Larsen, H.R. and Wratt, D.S. 2002. Barrier jets around the Southern Alps of New Zealand and their potential to enhance alpine rainfall. *Atmos. Res.*, 61, 277–98.
- Schaefer, J.T. 1986. *The dryline. Mesoscale Meteorology and Forecasting*, P.S. Ray, ed., Amer. Met. Soc., 549–72.
- Schultz, D.M., Weiss, C.C. and Hoffman, P.M. 2007. The synoptic regulation of dryline intensity. *Mon. Weath. Rev.*, 135, 1699–709.
- Smith, R.K., Reeder, M.J., May, P. and Richter, H. 2006. Low-level convergence lines over northeastern Australia. Part II: southerly disturbances. *Mon. Weath. Rev.*, 134, 3109–24.
- Spengler, T., Reeder, M.J. and Smith, R.K. 2005. The dynamics of heat lows in simple background flows. *Q. Jl R. Met. Soc.*, 131, 3147–65.
- Sultan, B., Janicot, S. and Drobinski, P. 2007. Characterization of the diurnal cycle of the West African monsoon around the monsoon onset. *Jnl climate*, 20, 4014–32.
- Sun, W.Y. and Ogura, Y. 1979. Boundary-layer forcing as a possible trigger to a squall-line formation. *J. Atmos. Sci.*, 36, 235–54.
- Sun, W.Y. and Wu, C.C. 1992. Formation and diurnal variation of the dryline. *J. Atmos. Sci.*, 49, 1606–19.
- Ziegler, C.L. and Hane, C.E. 1993. An observational study of the dryline. *Mon. Weath. Rev.*, 121, 1134–51.
- Ziegler, C.L., Martin, W.J. Pielke, R.A. and Walko, R.L. 1995. A modeling study of the dryline. *J. Atmos. Sci.*, 52, 263–85.

